

**Fig. 4.** Partial pressure at masses 2 and 16 as a function of crystal temperature for a heating rate of  $2 \text{ K s}^{-1}$  from a crystal covered with about  $0.85 \text{ ML}$  of surface-bound H and  $0.15 \text{ ML}$  of  $\text{CH}_3$ .

were carried out in the absence of bulk D or H but in the presence of surface-bound D or H. Adsorbed methyl radicals are produced by the dissociative chemisorption of  $17 \text{ kcal mol}^{-1} \text{ CH}_4$  on a clean surface. The surface was then exposed to molecular deuterium or hydrogen, which resulted in approximately  $0.85 \text{ ML}$  of adsorbed D or H atoms. The crystal temperature is then ramped at  $2 \text{ K s}^{-1}$ . The resulting thermal desorption experiment for the case of surface-bound H isotope is shown in Fig. 4. No methane was observed to desorb at any temperature. The hydrogen bound to the surface as well as the hydrogen produced from the decomposition of  $\text{CH}_3$  recombines and desorbs between 300 and 400 K. Carbon is observed by Auger spectroscopy to remain on the surface after heating to 500 K.

Mono-deuterated methane was formed solely by the reaction with bulk deuterium. The surface-bound D was unreactive with  $\text{CH}_3$ . The reaction likely proceeds by the direct recombination of a bulk D atom with  $\text{CH}_3$  because the interstitial octahedral site in which the D atom is bound (14) is directly beneath the threefold hollow surface site on which the  $\text{CH}_3$  species is bound (15). As the surface temperature is raised, the adsorbed D atom moves up toward the surface where it encounters the  $\text{CH}_3$  species. Because the D atom has the correct orientation required by the transition state for  $sp^3$  hybridization, it reacts with  $\text{CH}_3$ , immediately desorbing as  $\text{CH}_3\text{D}$ . The reaction of  $\text{CH}_3$  with a surface-bound D atom probably does not occur because access of the D atom to the  $\text{Ni}_3\text{-C}$  bond is blocked (17).

This result documents a new mechanism for a surface reaction, a reaction between an adsorbed and an absorbed species, and it unambiguously demonstrates the importance of bulk species as reactants in heterogeneous catalytic chemistry. This mechanism may be operable in many catalytic hydrogenation reactions.

## REFERENCES AND NOTES

- H. A. Smith, A. J. Chadwell, Jr., S. S. Kirsliis, *J. Phys. Chem.* **59**, 820 (1955).
- R. J. Kokes and P. H. Emmett, *J. Am. Chem. Soc.* **81**, 5032 (1959).
- \_\_\_\_\_, *ibid.* **82**, 4497 (1959).
- P. Gajardo, M. C. Lartiga, S. C. Droguett, *J. Phys. Chem.* **82**, 2323 (1978).
- I. Nakabayashi, T. Hisano, T. Terazawa, *J. Catal.* **58**, 74 (1979).
- M. Matsuyama *et al.*, *ibid.* **102**, 309 (1986).
- G. Alefeld and J. Völkl, Eds., *Hydrogen in Metals I & II* (Springer-Verlag, Berlin, 1986).
- K. J. Maynard *et al.*, *Faraday Discuss. Chem. Soc.* **91**, 437 (1991).
- A. D. Johnson, K. J. Maynard, S. P. Daley, Q. Y. Yang, S. T. Ceyer, *Phys. Rev. Lett.* **67**, 927 (1991).
- J. D. Beckerle, A. D. Johnson, Q. Y. Yang, S. T. Ceyer, *J. Chem. Phys.* **91**, 5756 (1986).
- J. D. Beckerle *et al.*, *ibid.* **93**, 4047 (1990).
- S. T. Ceyer, *Science* **249**, 133 (1990).
- M. B. Lee, Q. Y. Yang, S. T. Ceyer, *J. Chem. Phys.* **87**, 2724 (1987).
- A. D. Johnson, thesis, Massachusetts Institute of Technology, Cambridge (1991).
- S. T. Ceyer, *Langmuir* **6**, 82 (1990).
- A. Cornu and R. Massot, *Compilation of Mass Spectral Data* (Heyden, France, 1966).
- H. Wang and J. L. Whitten, *J. Chem. Phys.* **96**, 5529 (1992).
- Supported by the Department of Energy, Basic Energy Sciences (DE-FG02-89ER14035) and the Petroleum Research Fund (24882-AC5).

1 April 1992; accepted 20 May 1992

## Phototaxis of Spiral Waves

Mario Markus,\* Zsuzsanna Nagy-Ungvari,† Benno Hess

The drift of spiral waves toward regions of higher light intensity was observed experimentally in the ruthenium-catalyzed Belousov-Zhabotinsky reaction. A light gradient can thus be used to manipulate optical information in new computational systems based on photochemical media. The drift of a gradient that is rotationally invariant in space is three to four times as fast as that of a translationally invariant gradient. Simulations based on the use of a cellular automaton, which is made isotropic by a semirandom distribution of cells, are in agreement with the experimental results.

Spiral waves, rotating without a pacemaker and without attenuation, have been observed in different areas of science and in a variety of excitable media [for reviews, see (1)]. An area in an excitable medium may become excited by a suprathreshold perturbation; after excitation this area becomes refractory, slowly returning to the receptive state, where it can be excited again. Spiral waves in each of these media have several geometric and dynamic properties in common. Examples include heart muscle (2–4), the slime mold *Dyctostelium discoideum* (5), the retina (6), and the Belousov-Zhabotinsky (BZ) reaction (7, 8).

The BZ reaction, when catalyzed by the ruthenium bipyridyl complex,  $\text{Ru}(\text{bpy})_3^{2+}$ , is sensitive to visible light (9). The  $\text{Br}^-$  release in the reaction between  $\text{BrO}_3^-$  and the excited  $\text{Ru}(\text{bpy})_3^{2+}$  complex decreases the rate of autocatalysis, which is directly related to the velocity of wave propagation (7). In this context, it has been proposed that excitable media can be used in the implementation of new computational systems, such as associative memory devices (10) and learning machines (11). Searching for possibilities to manipulate spiral waves in such systems, researchers have

shown experimentally that, if light intensity varies in time with a period equal to that of the waves, these are linearly displaced ("resonance drift") (12). Brazhnik *et al.* (13) have theorized that the rotation of the spiral tip around its core in a spatial light gradient is equivalent to a periodic light modulation and thus should also lead to a spiral drift. They predicted that this drift should occur in the direction in which the critical curvature decreases, which according to our measurements corresponds to the direction of increasing light intensity. One should thus expect a "phototaxis" of the spirals. However, this idea has not been verified experimentally so far.

In our first attempts to measure this phototactic phenomenon, we encountered the difficulty of producing a constant light gradient (a linear dependence of the light intensity,  $I$ , on the spatial coordinate,  $x$ ). We transmitted the visible portion of the parallel light beam of a Cermax LX300 lamp through a slide with the photograph of a computer-generated gray-level function  $g(x)$  on it. A linear gray-level function  $g(x)$  yielded large deviations from linearity after photographing. However, we found that a linear  $I(x)$  can be obtained in our case by setting

$$g(x) = (1 - e^{-x/d}) / (1 - e^{-1}), \quad x \in [0, d]$$

Our experiments were performed with two types of spatial distributions of light intensity: (i) an axial gradient, where  $x$  is the

Max-Planck-Institut für Ernährungsphysiologie, Rheinlanddamm 201, W-4600 Dortmund, Germany.

\*To whom correspondence should be addressed.

†On leave from Lorand Eotvös University, Institute of Inorganic and Analytical Chemistry, Budapest, Hungary.

distance along a fixed direction of the petri dish and  $I(x)$  is constant perpendicular to this direction ( $d$  is the diameter of the dish); and (ii) a radial gradient, where  $x$  is the distance from the center of the dish and  $I(x)$

is constant for all angles of rotation around this center ( $d$  is the radius of the dish).

We used the following reagent concentrations:  $[\text{NaBrO}_3] = 0.2 \text{ M}$ ,  $[\text{H}_2\text{SO}_4] = 0.16 \text{ M}$ ,  $[\text{malonic acid}] = 0.03 \text{ M}$ ,  $[\text{bromo-}$

malonic acid] =  $0.09 \text{ M}$ , and  $[\text{Ru}(\text{bpy})_3\text{SO}_4] = 0.003 \text{ M}$ . The solution layers,  $0.3 \text{ mm}$  thick, were covered and thermostated to  $25.0^\circ \pm 0.1^\circ\text{C}$ . The temperature was held constant at different locations along the light gradient to exclude thermal effects. Light intensity was  $I = 0.1 \text{ W/m}^2$  for homogeneous illumination. For axial and radial light gradients, the intensity had this value at  $x = 0$  and increased linearly by  $1.2 \text{ W/m}^2$  every millimeter between  $x = 0$  and  $x = d$ . Spatial patterns were measured at  $460 \text{ nm}$  by a two-dimensional spectrophotometer combined with video imaging techniques, as given in (8). In the pictures shown here, white corresponds to  $\text{Ru}^{3+}$  (excited state) and black to  $\text{Ru}^{2+}$  (refractory and receptive states).

For simulations, we applied the cellular automaton as described in (14), which made use of a semirandom grid, to solve the long-lasting problem of wave-propagation anisotropy. Automata used earlier were not isotropic because periodic grids led to polygonal waves (15) or, at best, polygons with rounded corners (16); thus, wave curvature depended on the spatial direction. This could not be allowed here because of the essential role of curvature in the predicted drift. We adapted the isotropic automaton to the present work, making the assumption that light increases the refractory time. This is justified by the experimental evidence that  $\text{Br}^-$  is released during the photoexcitation of the  $\text{Ru}(\text{bpy})_3^{2+}$ -catalyzed BZ reaction (9, 10) and that  $\text{Br}^-$  prolongs recovery to the receptive state (7). The model parameters (14) were set as follows:  $m_0 = 5$ ,  $p = 2$ ,  $S_{\max} = 3$ ,  $\tau = 5$ . The refractory time is  $n = 5$  in the simulations with homogeneous illumination. For axial and radial gradients,  $n = 5$  at  $x = 0$  and increases linearly by  $\Delta n = 1$  every 13 cells between  $x = 0$  and  $x = d$ . As was the case in the experimental images, in the displays of our simulations black indicates the receptive state, and white indicates the excited state. However, refractory states are indicated by different levels of gray.

Figure 1 shows a time sequence of the experimentally observed behavior of a pair of spirals under an axial light gradient. Several phenomena can be seen. (i) In spite of the symmetric initial arrangement (Fig. 1A,  $t = 0$ ), symmetry is soon broken (Fig. 1B), one spiral (the left one here) becoming increasingly larger than the other one (Fig. 1C). (ii) The wavelength of the spiral increases after the loss of symmetry, because the motion in the light gradient considerably delays collision of the two spiral tips. (iii) After collision of the spirals at  $t = 9.3 \text{ min}$  (Fig. 1D) the smaller spiral disappears, a fragment of the larger spiral is cut off at the point of collision (Fig. 1, E and F), and this fragment grows until it dominates the

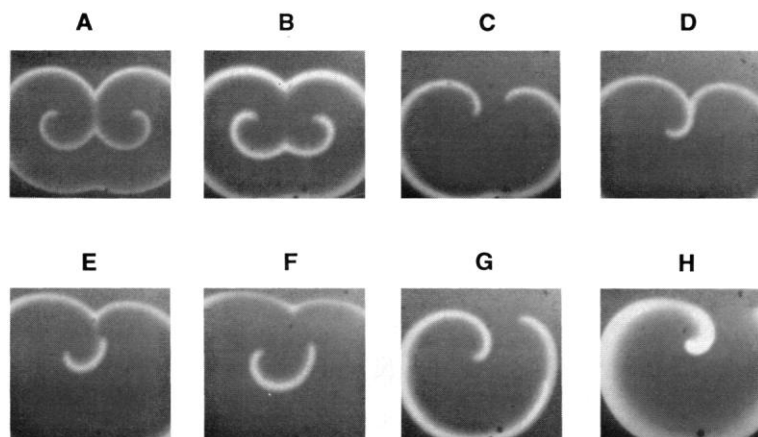


**Fig. 1.** Experimental results. (A) Homogeneous light intensity; (B through H) light intensity increases linearly from the bottom to the top edges. Times (in minutes): 0 (A), 6.92 (B), 8.7 (C), 9.3 (D), 9.51 (E), 9.81 (F), 14.66 (G), and 23.26 (H). Image area:  $0.90 \text{ cm}$  by  $0.90 \text{ cm}$ .

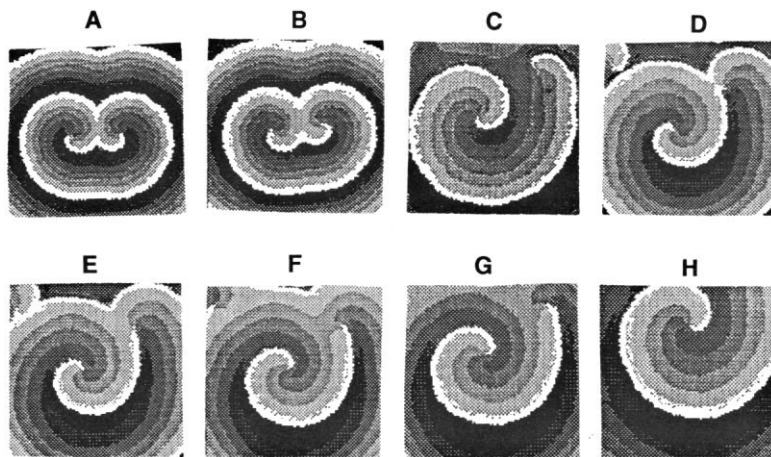
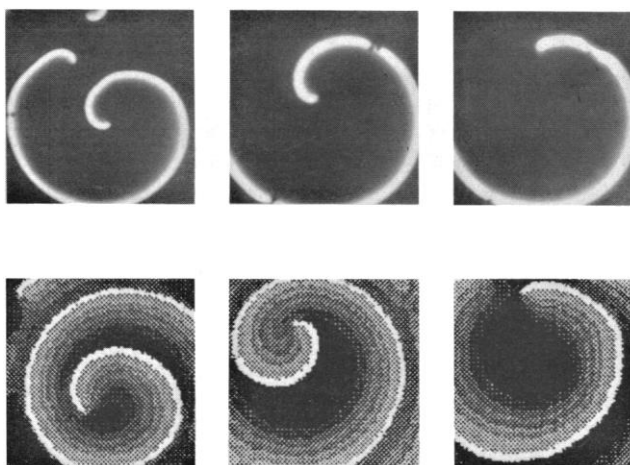


**Fig. 2.** Simulation of the time sequence shown in Fig. 1 based on the use of the cellular automaton described in (14). Times (in iteration steps): 0 (A), 29 (B), 45 (C), 50 (D), 51 (E), 53 (F), 70 (G), and 109 (H). Display size:  $108 \text{ cells}$  by  $108 \text{ cells}$ .

**Fig. 3. (Top)** Experimental results for light intensity increasing linearly from the center to the border of the petri dish. Times (in minutes) from left to right: 0, 11.42, and 15.17. Image area:  $0.90 \text{ cm}$  by  $0.90 \text{ cm}$ . **(Bottom)** Simulations with the automaton described in (14). Times (in iteration steps) from left to right: 0, 25, and 34. Display size:  $108 \text{ cells}$  by  $108 \text{ cells}$ .



whole medium (Fig. 1, G and H); thus, from two spirals only one is left. (iv) The spirals drift toward higher light intensity, as predicted in (13), which can be seen from a comparison of the tip position at different times; the drift is screw-like, as it is accompanied by the rotating motion of the spiral tip. The mean velocity of the drift has one component in the direction of the light gradient and another one perpendicular to it. The mean drift velocity, which can be estimated by comparing Fig. 1G with Fig. 1H, is  $1.7 \times 10^{-2}$  cm/min. (v) Strong deviations from the Archimedean spiral occur, the wavelength becoming larger in the regions with lower light intensity.

Figure 2 shows the automaton simulations corresponding to the experiments of Fig. 1. In agreement with these experimental results, the simulations yield instability in which the symmetry of the spiral pair is lost; the wavelength is enhanced; a spiral pair is transformed into a single spiral; there is spiral drift; and the system deviates from the Archimedean shape.

In order to quantify the automaton results, it is necessary that the iteration step and the length of a cell be expressed in physical time and space units. This can be done by comparing the period  $T$  and the wavelength  $\lambda$  of a spiral in homogeneous light (Figs. 1A and 2A). Experiments yield  $T = 1.5$  min and  $\lambda = 0.23$  cm. Simulations render  $T = 7$  steps and  $\lambda = 31$  cells. Thus, one iteration step corresponds to 0.21 min and one cell automaton is  $7.4 \times 10^{-3}$  cm long. The mean drift velocity, estimated by comparing Fig. 2G with Fig. 2H, is 0.53 cells per step, which in physical units is  $1.9 \times 10^{-2}$  cm/min, in good agreement with the experimental value of  $1.7 \times 10^{-2}$  cm/min obtained above.

An experiment with a radial gradient is shown in the upper pictures of Fig. 3; the corresponding automaton simulations are displayed below. Both in experiments and in simulations we observed that spirals straighten up, leading to uncurled wave ends. Also, we observed partial breaking of wave fronts into pieces. At the end of the experiment the mean drift velocity of the spiral tip is  $5.9 \times 10^{-2}$  cm/min, 3.5 times the velocity for the axial light gradient (Fig. 1). This is in good agreement with simulations. In fact, comparing the last two figures in the lower part of Fig. 3, we obtain a velocity of 2.1 cells per step, four times the value obtained for the axial gradient. This velocity enhancement is attributable to the fact that the spiral tip, while it is driven out of the medium in a screw-like fashion, encounters more often a driving light gradient when this gradient is radial than when the gradient points solely in one spatial direction.

The results presented here are at least qualitatively related to wave dynamics in heart muscle, as excitable media share some

common fundamental properties (1, 3). Measurements in vivo (2) and in isolated heart muscle (4) indicate that spiral formation is the cause of arrhythmic diseases. Moreover, simulations of heart muscle with partial differential equations (17) have shown that a gradient of refractoriness causes spiral drift. It has been suggested (18) that the traditional treatment, which consists of depolarizing shocks in the kilovolt range, may be replaced by implantable defibrillators operating at much lower potentials. In addition, the ability to control spiral drift in excitable media may find application in parallel processing with photochemical computational devices (9–11, 19).

#### REFERENCES AND NOTES

1. A. V. Holden, M. Markus, H. G. Othmer, Eds., *Nonlinear Wave Processes in Excitable Media* (Plenum, New York, 1990); H. L. Swinney and V. I. Krinsky, Eds., *Waves and Patterns in Chemical and Biological Media* [*Physica D* 49 (nos. 1 and 2) (1991)].
2. K. I. Allestie, F. I. M. Bonke, F. J. G. Schopman, *Circ. Res.* 33, 54 (1973); *ibid.* 39, 168 (1976); *ibid.* 41, 9 (1977).
3. J. Jalife, Ed., *Mathematical Approaches to Cardiac Arrhythmias* [*Ann. N.Y. Acad. Sci.* 561 (1990)].
4. J. M. Davidenko, P. Kent, J. Jalife, *Physica D* 49, 182 (1991); J. M. Davidenko, A. M. Pertsov, R. Salomonsz, W. Baxter, J. Jalife, *Nature* 355, 349 (1992).

5. G. Gerisch, *Naturwissenschaften* 58, 430 (1971); P. Foerster, S. C. Müller, B. Hess, *Development* 109, 11 (1990).
6. A. Gorelova and J. Bures, *J. Neurobiol.* 14, 353 (1983).
7. R. J. Field and M. Burger, Eds., *Oscillations and Traveling Waves in Chemical Systems* (Wiley, New York, 1985).
8. S. C. Müller, Th. Plesser, B. Hess, *Science* 230, 661 (1985); P. Foerster, S. C. Müller, B. Hess, *ibid.* 241, 685 (1988).
9. L. Kuhnert, *Nature* 319, 393 (1986).
10. ———, K. I. Agladze, V. I. Krinsky, *ibid.* 337, 244 (1989).
11. Ch. Zülicke, W. Ebeling, L. Schimansky-Geier, *BioSystems* 22, 261 (1989).
12. K. I. Agladze, V. A. Davydov, A. S. Mikhailov, *JETP Lett.* 45, 768 (1988).
13. P. K. Brazhnik *et al.*, *Izv. Vyssh. Uchebn. Zaved. Radiofiz.* 31, 574 (1988).
14. M. Markus and B. Hess, *Nature* 347, 56 (1990).
15. B. F. Madore and W. L. Freedman, *Science* 222, 615 (1983); A. T. Winfree, E. M. Winfree, H. Seifert, *Physica D* 17, 109 (1985).
16. M. Gerhardt and H. Schuster, *Physica D* 36, 209 (1989); ———, J. J. Tyson, *Science* 247, 1563 (1990).
17. A. V. Panfilov and B. N. Vasiev, *Chaos, Solitons, Fractals* 1, 119 (1991).
18. A. T. Winfree, *Ann. N.Y. Acad. Sci.* 561, 190 (1990).
19. H. Haken, *J. Chem. Phys.* 84, 1289 (1988); *Z. Phys.* 470, 121 (1988); W. Ebeling, *J. Stat. Phys.* 45, 891 (1986).
20. This work is part of Study Project PS\* 0303 of the Commission of the European Communities (Brussels). We thank W.-D. Sponheimer and H. Schepers for computational assistance and J. Ungvarai for help in carrying out the experiments.

15 January 1992; accepted 7 May 1992

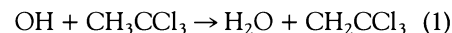
## Kinetics of the OH Reaction with Methyl Chloroform and Its Atmospheric Implications

Ranjit K. Talukdar, Abdelwahid Mellouki,\* Anne-Marie Schmoltner, Thomas Watson, Stephen Montzka, A. R. Ravishankar†

The rate coefficients for the reaction of hydroxyl (OH) radicals with methyl chloroform ( $\text{CH}_3\text{CCl}_3$ ) were measured between 243 and 379 kelvin with the pulsed photolysis–laser-induced fluorescence method. The measured rate coefficients at 298 and 277 kelvin were  $\sim 20$  and  $\sim 15\%$ , respectively, lower than earlier values. These results will increase the tropospheric OH concentrations derived from the  $\text{CH}_3\text{CCl}_3$  budget analysis by  $\sim 15\%$ . The predicted atmospheric lifetimes of species whose main loss process is the reaction with OH in the troposphere will be lowered by 15% with consequent changes in their budgets, global warming potentials, and ozone depletion potentials.

Methyl chloroform ( $\text{CH}_3\text{CCl}_3$ ) is exclusively man-made. Its rate of release into the atmosphere can be accurately estimated from industry production figures (1), and its atmospheric loss is due primarily to reaction with OH radicals. [Recently, oceanic consumption has been identified as an additional small loss process accounting for about 7% of the total  $\text{CH}_3\text{CCl}_3$  removal (2).] Therefore, measurements of atmospheric  $\text{CH}_3\text{CCl}_3$  concentrations have been used to deduce globally averaged tropospheric OH concentrations (3), which in turn are used to calculate atmospheric life-

times of species such as methane ( $\text{CH}_4$ ) and haloethanes, which are used as chlorofluorocarbon (CFC) substitutes. The OH concentrations calculated from the  $\text{CH}_3\text{CCl}_3$  budget analysis critically depend on the rate coefficient,  $k_1$ , for the reaction



The generally accepted value of  $k_1$  (4, 5) is based on the results of Kurylo *et al.* (6) and Jeong and Kaufman (7), which are in good agreement with each other between 278 and 363 K. Investigations carried out earlier than these two studies reported significantly